Validating a thermodynamic model for self-pressurization in liquid hydrogen tanks using novel tank trailer data

Christian Wolf[1,2], Daniel Siebe[1], Laura Stops[1], Alexander Alekseev[1,2], Sebastian Rehfeldt[1] and Harald Klein[1]

[1]Technical University of Munich, TUM School of Engineering and Design, Department of Energy and Process Engineering, Institute of Plant and Process Technology, Garching, Germany

[2]Linde GmbH, Clean Energy Technologies R&D, Pullach, Germany

E-mail: christian.georg.wolf@tum.de

Abstract. To ensure the safe and efficient operation of the liquid hydrogen (LH_2) infrastructure, it is crucial to understand the underlying thermodynamic processes. The self-pressurization rate of LH_2 tanks due to heat inleak is important for safe operation. A variety of models for this phenomenon is proposed in the literature, but published experimental data are sparse, and mostly comes from stationary LH_2 tanks. In this work, novel experimental data on the self-pressurization of an LH_2 trailer in operation is presented. The unique benefit of this pressure data lies in the fact that the phases in the trailer can be either in equilibrium, when the trailer is on the road and the phases are mixed due to the dynamic movements, or in non-equilibrium, when the trailer is parked. This enables the study of the different self-pressurization rates for both scenarios. The presented experimental data are used to validate a thermodynamic model based on the literature. The insights gained from this work support the development of universally applicable models for a safe operation of LH_2 tanks.

1 Introduction

The demand for liquid hydrogen (LH_2) has been rising in recent years, driven in part by emerging applications in the clean energy sector, such as CO_2-emission free heavy-duty transportation. The increasing production of LH_2 requires an efficient and safe LH_2 supply chain. The self-pressurization of LH_2 storage tanks and LH_2 trailers due to heat inleak is important for safe operation, but developing an accurate and universally applicable model of this phenomenon is challenging due to the limited availability of published validation data. Most data come from stationary LH_2 storage tank experiments, where even modeling the heat inleak already relies on heat transfer correlations or additional complex boil-off tests. Data from mobile systems such as LH_2 trailers are rarely available.

2 Methodology

An opportunity for detailed observation emerged during the commissioning phase of an LH_2 trailer, where the thermal insulation performance did not meet specifications. It is presumed that the faulty thermal insulation resulted from a manufacturing defect, causing up to 10 times higher heat inleak than usual. For further testing, this trailer was equipped with a pressure data logger. The data logger of the type Madgetech PR1000Ex-300psi measures the pressure in the ullage with a frequency of $\frac{1}{\text{min}}$ and stores the data in local memory. The trailer was in test operation for several weeks, distributing LH_2 from a hydrogen liquefaction plant to the consumers. The pressure data from the test operation was combined with weighing data from a vehicle scale at the hydrogen liquefaction plant, and with data from

an onboard flow meter to measure the unloaded LH_2 at the consumers. Knowing the net weight of the empty trailer, the total mass M of loaded hydrogen after filling can be determined with the vehicle scale. The onboard flow meter measures the mass flow $\dot{M}_{\mathrm{out}}$ exiting the trailer during unloading. Its integrated electronics include a totalizer function which provides the total unloaded mass ΔM_{out} at the end of the consumer delivery. The fact that the trailer is sometimes in motion (driving) and sometimes stationary (parked), in combination with the unusually high heat inleak, provides a unique opportunity to study the self-pressurization phenomenon. An exemplary pressure curve over a timespan of 22 h of the observed trailer during a part of the distribution is shown in Figure 1. This curve was not taken from one of the provided data sets.

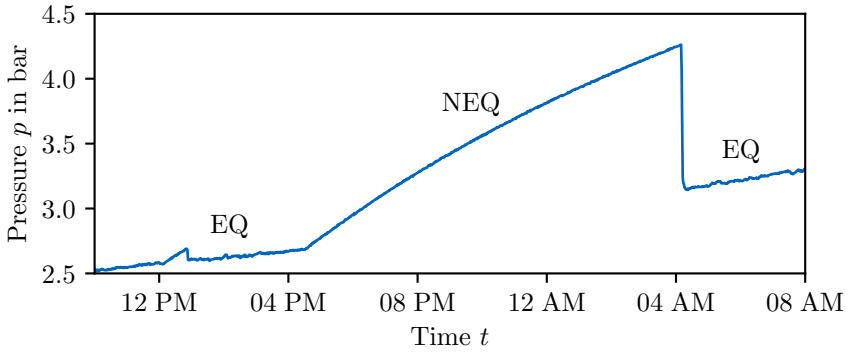

Figure 1: Exemplary pressure curve over a time of the LH_2 trailer.

When the trailer drives on the road until approximately 04 PM, the dynamic driving leads to acceleration forces acting on the hydrogen in the trailer. The gaseous hydrogen (GH_2) and the LH_2 in the trailer are mixed and phase equilibrium (EQ) can be assumed. In EQ, the temperature T_{gas} of the GH_2, and the temperature T_{liq} of the LH_2 are equal to the saturation temperature T_{sat} of the prevailing pressure p in the trailer ($T_{\mathrm{gas}} = T_{\mathrm{liq}} = T_{\mathrm{sat}}$). Afterwards, the trailer is parked for the night rest. During this time, the trailer is stationary and due to the heat flow $\dot{Q}_{\mathrm{amb}}$ from the ambience, non-equilibrium (NEQ) is induced. As a result, the temperature of the GH_2 increases above the temperature of the LH_2 ($T_{\mathrm{gas}} > T_{\mathrm{sat}} > T_{\mathrm{liq}}$), and the pressure rise over time is multiple times faster than in EQ. When the trailer departs on the next morning just after 04 AM, the GH_2 and the LH_2 are mixed again due to the dynamic driving and EQ is re-established. This process is called *Sloshing* and leads to a pressure decrease, as visible in Figure 1. During driving, EQ can be assumed again. In the whole process, the total mass M of the loaded hydrogen stays constant, as no hydrogen enters or exits the trailer. The total mass M of the loaded hydrogen is either known due to weighing, if the trailer did not supply a consumer since the departure from the hydrogen liquefaction plant, or it can be estimated from simulating the unloading process at the consumers. At a consumer, the total mass of loaded hydrogen reduces by the unloaded mass ΔM_{out}, and additional process-related losses which are obtained from simulations.

When the GH_2 and the LH_2 in the trailer are in EQ, the total density ϱ can be determined based on the trailer volume V:

$$\varrho = \frac{M}{V} \,. \tag{1}$$

The measured pressure p and the total density ϱ obtained from Equation (1) completely describe the thermodynamic state of the loaded hydrogen in EQ. Using the equations of state (EOS) from [1], the specific internal energy u can be determined:

$$u = u(p, \varrho) \,. \tag{2}$$

By formulating the energy balance between two separate points in time (t_1, t_2) in which the GH_2 and the LH_2 in the trailer are in EQ, the time-averaged heat flow $\dot{Q}_{\mathrm{amb}}$ from the ambience can be obtained:

$$\dot{Q}_{\mathrm{amb}} = M \cdot \frac{u_2 - u_1}{t_2 - t_1} \,. \tag{3}$$

Applying this straightforward approach on the available trailer data, the heat inleak can be obtained without the need of further correlations between the ambience, the wall, and the fluid. To study the NEQ self-pressurization in greater detail, 3 data sets from the observed trailer, listed in Table 1, are prepared.

Table 1: Boundary conditions and properties of the NEQ time span data used in the self-pressurization simulation.

Data set:	A	B	C
Heat inleak $\dot{Q}_{\mathrm{amb}}$	674 W	626 W	599 W
Initial pressure p_0	3.23 bar	2.44 bar	2.34 bar
Initial volumetric liquid fraction L_{f0}	58 %	40 %	78 %
Total mass M	2210 kg	1620 kg	3000 kg
Trailer volume V	$56.54\,\mathrm{m}^3$		
Trailer diameter D	$\approx 2.5\,\mathrm{m}$		

The values for the heat inleak in the data sets A and C in Table 1 are determined from a point in time t_1 in EQ before, and a point in time t_2 in EQ after the night rest. For data set B, both points in time t_1 and t_2 in EQ are taken from before the night rest. This approach is used because it is assumed that no complete sloshing occurs at the end of data set B, and therefore, full EQ is not reached. The trailer volume V is known, but the trailer diameter D needs to be estimated. Modeling the trailer as a horizontal cylinder, an estimated trailer length $L \approx 11.52\,\mathrm{m}$ can be determined using the given trailer volume, and the estimated trailer diameter D.

The raw experimental data sets with time steps of 5 min are listed in Table 2 – Table 4 in Appendix A. The complete data sets, with time steps of 1 min, resulting from the full measuring frequency of the pressure data logger, are available upon request. All pressure values presented in this work are given in bar absolute.

3 Thermodynamic model

In the thermodynamic model of the trailer during the NEQ self-pressurization due to heat inleak, for each of the GH_2 phase and the LH_2 phase, an ideally mixed control volume is assumed. The phases are separated by a massless, infinitesimally thin, saturated film. The pressure p is assumed to be spatially uniform throughout the trailer, and the isomeric form of the hydrogen is assumed to be 100% parahydrogen at all times. A schematic of the thermodynamic model is shown in Figure 2.

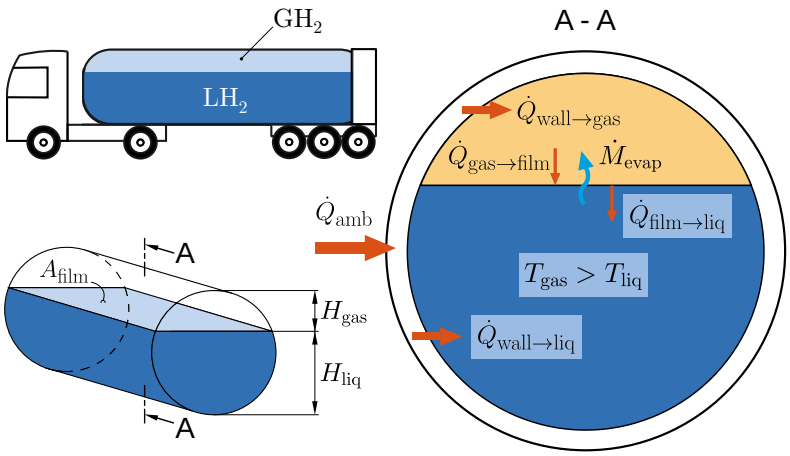

Figure 2: Schematic of the thermodynamic model of the trailer during the NEQ self-pressurization due to heat inleak, with the subcooled LH_2 phase indicated in blue, and the superheated GH_2 phase indicated in yellow.

In the following equations, only the heat flows entering the control volumes, and the heat flows and mass flows exchanged between the control volumes, as shown in Figure 2, are presented. The complete model setup includes a differential-algebraic system with the energy and mass balances of both control volumes and the complete trailer, and is not presented in this work.

The inner surface area A_{wall} of the trailer is given by

$$A_{\mathrm{wall}} = 2 \cdot \frac{D^2 \cdot \pi}{4} + D \cdot \pi \cdot L \,. \tag{4}$$

The heat flow $\dot{Q}_{\mathrm{amb}}$ from the ambience is split up, depending on the inner surface area A_{gas} in contact with GH_2, and the inner surface area A_{liq} in contact with LH_2:

$$\dot{Q}_{\mathrm{wall}\to\mathrm{gas}} = \dot{Q}_{\mathrm{amb}} \cdot \frac{A_{\mathrm{gas}}}{A_{\mathrm{wall}}} \tag{5}$$

$$\dot{Q}_{\mathrm{wall}\to\mathrm{liq}} = \dot{Q}_{\mathrm{amb}} \cdot \frac{A_{\mathrm{liq}}}{A_{\mathrm{wall}}} \,. \tag{6}$$

The heat flow $\dot{Q}_{\mathrm{wall}\to\mathrm{gas}}$ enters the GH_2 and the heat flow $\dot{Q}_{\mathrm{wall}\to\mathrm{liq}}$ enters the LH_2. The heat flow $\dot{Q}_{\mathrm{gas}\to\mathrm{film}}$ from the GH_2 to the saturated film, and the heat flow $\dot{Q}_{\mathrm{film}\to\mathrm{liq}}$ from the saturated film to the LH_2 are determined as follows:

$$\dot{Q}_{\mathrm{gas}\to\mathrm{film}} = \alpha_{\mathrm{gas}} \cdot A_{\mathrm{film}} \cdot (T_{\mathrm{gas}} - T_{\mathrm{film}}) \tag{7}$$

$$\dot{Q}_{\mathrm{film}\to\mathrm{liq}} = \alpha_{\mathrm{liq}} \cdot A_{\mathrm{film}} \cdot (T_{\mathrm{film}} - T_{\mathrm{liq}}) \,. \tag{8}$$

The convective heat transfer coefficient α_{gas} at the boundary of the saturated film and the GH_2, and the convective heat transfer coefficient α_{liq} at the boundary of the saturated film and the LH_2 are determined using correlations. The surface area A_{film} of the saturated film changes with the liquid level of the trailer. The driving force of the heat flow between the control volumes is the difference between the temperature T_{gas} of the GH_2, and the temperature T_{liq} of the LH_2. The temperature T_{film} of the film is the saturation temperature T_{sat} which corresponds to the prevailing pressure p, and can be determined using the EOS:

$$T_{\mathrm{film}} = T_{\mathrm{sat}}(p) \,. \tag{9}$$

To determine the heat transfer coefficients, a correlation proposed in [2] is used, comprising the thermal conductivity λ_{gas}, the height H_{gas} of the control volume, and the Rayleigh number Ra_{gas} of the GH_2, and the thermal conductivity λ_{liq}, the height H_{liq} of the control volume, and the Rayleigh number Ra_{liq} of the LH_2.

$$\alpha_{\mathrm{gas}} = k_{\mathrm{gas}} \cdot \frac{\lambda_{\mathrm{gas}}}{H_{\mathrm{gas}}} \cdot 0.27 \left(Ra_{\mathrm{gas}}\right)^{0.25} \tag{10}$$

$$\alpha_{\mathrm{liq}} = k_{\mathrm{liq}} \cdot \frac{\lambda_{\mathrm{liq}}}{H_{\mathrm{liq}}} \cdot 0.27 \left(Ra_{\mathrm{liq}}\right)^{0.25} \,. \tag{11}$$

It is stated that the calibration constants k_{gas} and k_{liq} shall be adjusted to the observed system, in [2] the values $k_{\mathrm{gas}} = k_{\mathrm{liq}} = 0.055$ are used. The evaporation mass flow $\dot{M}_{\mathrm{evap}}$ is determined from an energy balance around the massless, saturated film:

$$\dot{M}_{\mathrm{evap}} = \frac{\dot{Q}_{\mathrm{gas}\to\mathrm{film}} - \dot{Q}_{\mathrm{film}\to\mathrm{liq}}}{\Delta h} \,. \tag{12}$$

The specific enthalpy difference Δh depends on the ratio of the heat flows $\dot{Q}_{\mathrm{gas}\to\mathrm{film}}$ and $\dot{Q}_{\mathrm{film}\to\mathrm{liq}}$:

$$\Delta h = \begin{cases} h'' - h_{\mathrm{liq}} & \text{if} \quad \dot{Q}_{\mathrm{gas}\to\mathrm{film}} > \dot{Q}_{\mathrm{film}\to\mathrm{liq}} \\ h_{\mathrm{gas}} - h' & \text{if} \quad \dot{Q}_{\mathrm{gas}\to\mathrm{film}} < \dot{Q}_{\mathrm{film}\to\mathrm{liq}} \,. \end{cases} \tag{13}$$

The first case of Equation (13) describes evaporation, where the specific enthalpy h_{liq} of the LH_2, and the specific enthalpy h'' of saturated GH_2 are used. The second case of Equation (13) describes condensation, where the specific enthalpy h_{gas} of the GH_2 and the specific enthalpy h' of saturated LH_2 are used. The case of condensation results in a negative value for $\dot{M}_{\mathrm{evap}}$ in Equation (12), indicating the opposite direction of the mass flow in Figure 2.

Thermodynamic property data in this work is obtained from REFPROP [3]. The thermodynamic model is implemented in MATLAB [4] which is linked to the REFPROP database via a subroutine [5].

4 Results and conclusion

For the simulation of the self-pressurization in the data sets A, B, and C, the thermodynamic model was initialized with superheated GH_2 with a temperature difference $\Delta T_{gas} = 3\,K$ above saturation temperature (based on [2]), and with subcooled LH_2 with a temperature difference $\Delta T_{liq} = 0.5\,K$ below saturation temperature (to ensure the LH_2 remains subcooled). The simulation results are shown in Figure 3. The simulations with the calibration constants $k_{gas} = k_{liq} = 0.055$ as used in [2] show a maximum deviation of less than 0.5 bar in the observed time span of 12 h. However, to be able to minimize the deviation in simulations for longer time spans, the slope of the simulated and measured pressure curves need to match. To achieve this, the calibration constants $k_{gas} = k_{liq} = 0.04$ are proposed for the observed trailer, the parallel slopes at the end of the simulated and measured pressure curve are indicated in red in Figure 3c.

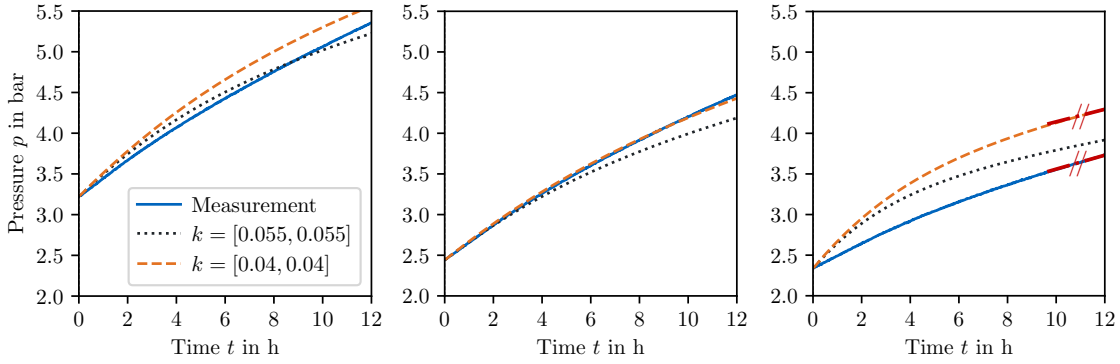

(a) Data set A with $L_{f0} = 58\,\%$. (b) Data set B with $L_{f0} = 40\,\%$. (c) Data set C with $L_{f0} = 78\,\%$.

Figure 3: Simulated self-pressurization with $k = [k_{gas}, k_{liq}]$ compared to the measurement data sets.

Further simulations show that the accuracy does not improve when adjusting the calibration constants independently ($k_{gas} \neq k_{liq}$). Therefore, a single calibration constant $k_{gas} = k_{liq} = k$ already provides the best achievable accuracy with the presented model. At a higher initial volumetric liquid fraction L_{f0} (data set C), the simulated pressure rise is overestimated, while at a lower initial volumetric liquid fraction L_{f0} (data set B), the simulation underestimates the pressure rise.

Overall, the accuracy of the simulation is sufficient to support the safe operation of LH_2 trailers. The advantage of the straightforward thermodynamic model is its universal applicability to a broader range of different LH_2 tank sizes and geometries.

Acknowledgments

The authors gratefully acknowledge the financial support of the project "TransHyDE_FP4" (03HY204F) by the German Federal Ministry of Research, Technology and Space (BMFTR) and the project supervision by the project management organization Projektträger Jülich (PtJ). We thank Lars Tilsner, Jörg Mickan, Frank Philipp, and Walther Ambros for their support and the contribution to the generation of the data.

References

[1] Leachman J W, Jacobsen R T, Penoncello S G and Lemmon E W 2009 Fundamental Equations of State for Parahydrogen, Normal Hydrogen, and Orthohydrogen *J. Phys. Chem. Ref. Data* **38** 721–748
[2] Matveev K I and Leachman J W 2023 The Effect of Liquid Hydrogen Tank Size on Self-Pressurization and Constant-Pressure Venting *Hydrogen* **4** 444–455
[3] Lemmon E W, Bell I H, Huber M L and McLinden M O 2018 NIST Standard Reference Database 23: Reference Fluid Thermodynamic and Transport Properties-REFPROP, Version 10.0
[4] The MathWorks Inc 2022 9.12.0.2039608 (R2022a) Update 5
[5] NIST 2019 Linking REFPROP w. other apps. URL `https://trc.nist.gov/refprop/LINKING/Linking.htm`

A Experimental data sets

On the following pages, the raw measurement data of the self-pressurization of the LH_2 trailer is provided.

Table 2: Measurement data of data set A with the simulated loaded hydrogen mass $M_A = 2210\,\text{kg}$.

Pressure p in bar	Time t in min	Pressure p in bar	Time t in min	Pressure p in bar	Time t in min	Pressure p in bar	Time t in min
3.110	0	3.495	240	4.296	480	4.951	720
3.116	5	3.515	245	4.313	485	4.959	725
3.123	10	3.539	250	4.322	490	4.972	730
3.130	15	3.553	255	4.335	495	4.986	735
3.140	20	3.569	260	4.352	500	4.996	740
3.144	25	3.590	265	4.366	505	5.018	745
3.154	30	3.611	270	4.386	510	5.023	750
3.154	35	3.627	275	4.397	515	5.036	755
3.165	40	3.649	280	4.410	520	5.048	760
3.168	45	3.664	285	4.427	525	5.060	765
3.170	50	3.682	290	4.439	530	5.077	770
3.179	55	3.699	295	4.452	535	5.082	775
3.160	60	3.720	300	4.469	540	5.098	780
3.177	65	3.738	305	4.480	545	5.116	785
3.180	70	3.752	310	4.495	550	5.124	790
3.177	75	3.770	315	4.504	555	5.136	795
3.182	80	3.791	320	4.524	560	5.145	800
3.186	85	3.803	325	4.537	565	5.163	805
3.188	90	3.824	330	4.549	570	5.171	810
3.194	95	3.844	335	4.561	575	5.184	815
3.197	100	3.852	340	4.576	580	5.200	820
3.189	105	3.872	345	4.589	585	5.210	825
3.213	110	3.887	350	4.608	590	5.221	830
3.231	115	3.906	355	4.619	595	5.232	835
3.199	120	3.920	360	4.630	600	5.247	840
3.212	125	3.937	365	4.642	605	5.261	845
3.213	130	3.952	370	4.655	610	5.267	850
3.228	135	3.972	375	4.666	615	5.280	855
3.223	140	3.983	380	4.687	620	5.292	860
3.226	145	4.006	385	4.700	625	5.304	865
3.227	150	4.021	390	4.717	630	5.314	870
3.239	155	4.029	395	4.727	635	5.329	875
3.248	160	4.050	400	4.738	640	5.340	880
3.229	165	4.067	405	4.750	645	5.352	885
3.240	170	4.076	410	4.767	650	5.363	890
3.250	175	4.100	415	4.783	655	5.376	895
3.276	180	4.114	420	4.795	660	5.105	900
3.289	185	4.132	425	4.811	665	3.941	905
3.307	190	4.142	430	4.820	670	3.892	910
3.326	195	4.158	435	4.837	675	3.902	915
3.344	200	4.174	440	4.852	680	3.895	920
3.365	205	4.190	445	4.854	685	3.898	925
3.380	210	4.206	450	4.871	690	3.899	930
3.403	215	4.224	455	4.882	695	3.919	935
3.422	220	4.234	460	4.899	700	3.942	940
3.440	225	4.250	465	4.912	705	3.949	945
3.455	230	4.263	470	4.924	710		
3.479	235	4.283	475	4.940	715		

Table 3: Measurement data of data set B with the simulated loaded hydrogen mass $M_B = 1620\,\text{kg}$.

Pressure p in bar	Time t in min	Pressure p in bar	Time t in min	Pressure p in bar	Time t in min	Pressure p in bar	Time t in min
2.354	0	2.932	240	3.651	480	4.249	720
2.355	5	2.949	245	3.668	485	4.260	725
2.362	10	2.974	250	3.685	490	4.274	730
2.371	15	2.987	255	3.694	495	4.281	735
2.378	20	3.002	260	3.707	500	4.295	740
2.385	25	3.022	265	3.718	505	4.309	745
2.389	30	3.036	270	3.732	510	4.314	750
2.391	35	3.054	275	3.746	515	4.326	755
2.391	40	3.066	280	3.763	520	4.341	760
2.397	45	3.084	285	3.772	525	4.348	765
2.398	50	3.100	290	3.787	530	4.362	770
2.401	55	3.113	295	3.796	535	4.370	775
2.398	60	3.133	300	3.811	540	4.383	780
2.407	65	3.153	305	3.824	545	4.394	785
2.410	70	3.165	310	3.840	550	4.407	790
2.425	75	3.182	315	3.853	555	4.412	795
2.422	80	3.199	320	3.866	560	4.424	800
2.420	85	3.210	325	3.873	565	4.444	805
2.438	90	3.229	330	3.882	570	4.437	810
2.433	95	3.243	335	3.902	575	4.458	815
2.437	100	3.255	340	3.916	580	4.470	820
2.455	105	3.271	345	3.923	585	4.483	825
2.478	110	3.289	350	3.934	590	4.494	830
2.492	115	3.303	355	3.945	595	4.505	835
2.507	120	3.321	360	3.964	600	4.514	840
2.530	125	3.330	365	3.977	605	4.525	845
2.541	130	3.343	370	3.985	610	3.411	850
2.561	135	3.356	375	3.995	615	3.393	855
2.577	140	3.374	380	4.010	620	3.387	860
2.600	145	3.388	385	4.023	625		
2.617	150	3.406	390	4.040	630		
2.634	155	3.419	395	4.045	635		
2.652	160	3.436	400	4.062	640		
2.666	165	3.444	405	4.075	645		
2.687	170	3.462	410	4.082	650		
2.705	175	3.477	415	4.094	655		
2.724	180	3.490	420	4.107	660		
2.741	185	3.507	425	4.120	665		
2.765	190	3.516	430	4.130	670		
2.773	195	3.533	435	4.143	675		
2.794	200	3.540	440	4.152	680		
2.814	205	3.561	445	4.164	685		
2.830	210	3.568	450	4.174	690		
2.846	215	3.589	455	4.188	695		
2.869	220	3.597	460	4.197	700		
2.887	225	3.612	465	4.212	705		
2.904	230	3.632	470	4.222	710		
2.919	235	3.643	475	4.240	715		

Table 4: Measurement data of data set C with the measured loaded hydrogen mass $M_C = 3000\,\text{kg}$.

Pressure p in bar	Time t in min	Pressure p in bar	Time t in min	Pressure p in bar	Time t in min	Pressure p in bar	Time t in min	Pressure p in bar	Time t in min
2.180	0	2.276	250	2.617	500	3.153	750	3.570	1000
2.175	5	2.281	255	2.630	505	3.168	755	3.573	1005
2.183	10	2.292	260	2.647	510	3.177	760	3.583	1010
2.189	15	2.293	265	2.662	515	3.183	765	3.591	1015
2.189	20	2.291	270	2.665	520	3.192	770	3.599	1020
2.194	25	2.296	275	2.675	525	3.200	775	3.606	1025
2.201	30	2.299	280	2.693	530	3.215	780	3.616	1030
2.199	35	2.302	285	2.706	535	3.220	785	3.626	1035
2.194	40	2.298	290	2.718	540	3.230	790	3.628	1040
2.195	45	2.306	295	2.733	545	3.238	795	3.638	1045
2.202	50	2.304	300	2.744	550	3.246	800	3.641	1050
2.201	55	2.305	305	2.753	555	3.250	805	3.652	1055
2.205	60	2.314	310	2.766	560	3.260	810	3.654	1060
2.202	65	2.322	315	2.781	565	3.271	815	3.664	1065
2.207	70	2.320	320	2.785	570	3.277	820	3.670	1070
2.219	75	2.327	325	2.801	575	3.288	825	3.680	1075
2.216	80	2.329	330	2.806	580	3.307	830	3.687	1080
2.211	85	2.332	335	2.822	585	3.310	835	3.694	1085
2.204	90	2.337	340	2.838	590	3.315	840	3.703	1090
2.215	95	2.321	345	2.843	595	3.322	845	3.710	1095
2.215	100	2.327	350	2.859	600	3.331	850	3.716	1100
2.215	105	2.326	355	2.865	605	3.338	855	3.724	1105
2.219	110	2.330	360	2.877	610	3.351	860	3.737	1110
2.222	115	2.329	365	2.888	615	3.357	865	3.740	1115
2.223	120	2.330	370	2.900	620	3.368	870	3.744	1120
2.221	125	2.337	375	2.912	625	3.377	875	3.753	1125
2.225	130	2.340	380	2.918	630	3.383	880	3.761	1130
2.232	135	2.333	385	2.932	635	3.393	885	3.771	1135
2.226	140	2.335	390	2.942	640	3.400	890	3.777	1140
2.223	145	2.351	395	2.952	645	3.407	895	3.789	1145
2.231	150	2.363	400	2.960	650	3.414	900	3.792	1150
2.232	155	2.373	405	2.976	655	3.431	905	3.794	1155
2.230	160	2.392	410	2.986	660	3.426	910	3.802	1160
2.236	165	2.404	415	2.997	665	3.441	915	3.811	1165
2.241	170	2.412	420	3.006	670	3.447	920	3.819	1170
2.242	175	2.429	425	3.017	675	3.449	925	3.824	1175
2.237	180	2.436	430	3.021	680	3.462	930	3.831	1180
2.248	185	2.452	435	3.032	685	3.467	935	3.836	1185
2.246	190	2.464	440	3.041	690	3.480	940	3.596	1190
2.265	195	2.479	445	3.052	695	3.490	945	2.806	1195
2.271	200	2.490	450	3.065	700	3.497	950	2.795	1200
2.279	205	2.506	455	3.073	705	3.502	955	2.797	1205
2.290	210	2.520	460	3.079	710	3.506	960	2.803	1210
2.307	215	2.533	465	3.093	715	3.516	965	2.799	1215
2.290	220	2.541	470	3.102	720	3.528	970	2.800	1220
2.271	225	2.557	475	3.115	725	3.531	975	2.804	1225
2.264	230	2.564	480	3.116	730	3.535	980	2.802	1230
2.270	235	2.582	485	3.132	735	3.550	985	2.814	1235
2.277	240	2.596	490	3.142	740	3.559	990	2.816	1240
2.290	245	2.607	495	3.147	745	3.564	995	2.821	1245